OPEN ACCESS

ACTA METALLURGICA SLOVACA

2026, VOL. 32, NO. 2, 116-123

RESEARCH PAPER

Formation and characterization of non-metallic inclusions in steel produced by melting secondary ferrous scrap in an electric arc furnace: A case study of AISI 1066 steel

Nozimjon Kholmirzaev[1], Nodir Turakhodjaev[1], Jamshidbek Khasanov[2], Chong Yang[3], Bekzod Yusupov[4], Shokhista Saidkhodjaeva[1], Abdujalol Bektemirov[5], Nargiza Sadikova[1], Zokirjon Nurdinov[1], Nuriddin Yusupov[2], Davronbek Juraboev[2], Bobomurod Nurmurodov[5]

[1]Department of Metal Technologies, Tashkent State Technical University, 100095 Tashkent, Uzbekistan
[2]Department of Mechanical Engineering, Andijan State Technical Institute, 170100, Andijan, Uzbekistan
[3]State Key Laboratory for Mechanical Behavior of Materials, Xi'an Jiaotong University, 710049 Xi'an P. R. China
[4]Department of Education Quality Control, Almalyk State Technical Institute, 110100, Tashkent region, Uzbekistan
[5]Laboratory of Mechanical Engineering and Materials Science, Uzbek-Japan Innovation Center of Youth, 100095 Tashkent, Uzbekistan

*Corresponding author: nozimjonxolmirzayev@gmail.com , tel.: +998911722233, Department of Metal Technologies, Faculty of Mechanical Engineering, Tashkent State Technical University named after Islam Karimov, 100095 Tashkent, Uzbekistan

Received: 27.04.2026
Accepted: 09.06.2026

ABSTRACT

This study investigated the formation of non-metallic inclusions and their characterization during the melting of AISI1066 steel from secondary metal scrap in an electric arc furnace. The analyses were carried out using scanning electron microscopy (SEM) and energy-dispersive X-ray spectroscopy (EDS). In addition, a deep learning-based segmentation method was applied to improve the identification of inclusions. The results confirmed a heterogeneous microstructure consisting of non-metallic inclusions dispersed within a Fe-based matrix. The size of the inclusions ranged from a few micrometers up to approximately 40 µm. The majority of inclusions were found in the 10–25 µm range. SEM analysis showed that the inclusions predominantly exhibit irregular and globular morphologies. EDS results confirmed that they consist of manganese sulfides (MnS), oxides (Al_2O_3 and SiO_2), and complex multi-phase particles. The elevated sulfur (S) (0.12 wt.%) and copper (Cu) (0.81 wt.%) contents in the investigated samples indicate that deoxidation and modification processes were not sufficiently effective. The deep learning-based model enabled accurate separation of non-metallic inclusions from the alloy composition. According to the model results, inclusions ≥30 µm primarily represent the oxide phase fraction, while fine inclusions <20 µm represent the sulfide phase fraction.

Keywords: non-metallic inclusions, scrap-based, inclusion size distribution, deep learning, oxide and sulfide, metallurgical cleanliness

INTRODUCTION

The physical–mechanical properties and service performance of steel components are directly dependent on the presence and distribution of non-metallic inclusions in their structure. Therefore, these inclusions are generally considered as factors that negatively affect the properties of steel [1–3].

Non-metallic inclusions in steels are classified into endogenous (such as sulfides, oxides, silicates, and similar compounds) and exogenous (originating from furnace lining, casting nozzles, ladles, mold mixtures, etc.) types [4,5]. This classification is based on their origin and formation mechanisms [6,7].

The size and distribution of non-metallic inclusions depend on the physicochemical processes occurring during solidification [8,9]. They form due to deoxidation products, slag entrapment, and chemical reactions during the steelmaking process [10–15].

One of the most widely used methods for producing high-quality steel is deoxidation using aluminum [16–20]. Because during the melting process, aluminum in the composition strongly binds with oxygen and forms Al_2O_3, and also binds other non-metallic elements to itself. As a result, it helps improve the cleanliness of steel. However, this method is not always fully effective. In addition, advanced industrial techniques such as secondary refining, argon stirring, and calcium modification are also applied to reduce the amount of non-metallic inclusions [21–34].

However, ensuring the quality of steel and its alloys during the melting of secondary metal resources is a complex process in itself [35,36]. This is because it is impossible to control secondary metal scrap and its composition. Elements such as Cu, Sn, As, and Sb are also present in secondary metal and remain in the alloy during melting. As a result, they adversely affect the alloy's mechanical properties and technological characteristics [37]. Therefore, steel production based on secondary scrap is more complex compared to primary production methods and is characterized by a lower quality of the resulting alloy.

Dobosz et al. [37] found that, in technology based on producing steel from secondary metal resources, elements such as Cu, Sn, As, and Sb always remain in the composition of steel and its alloys. It is impossible to transfer them into the slag during the melting process. As a result, they form weak compounds at the grain boundaries. This leads to deterioration of mechanical properties. Dworak et al. [38] observed that the proportion of low-quality scrap increases over time due to the accumulation of elements such as Cu, Sn, Cr, Ni, and Mo, which necessitates improved refining or additional purification technologies. Wang et al. [39] found that in Al-containing high-entropy alloys (HEAs), Al_2O_3 inclusions initially form in the liquid phase and act as nucleation sites for AlN, resulting in Al_2O_3–AlN agglomerates. Qiao et al. [40] found that, based on the results of the conducted study, MgO–Al_2O_3 inclusions were initially formed in 42CrMo4 steel. Then, under the effect of Ca addition as a slag-forming agent during the melting process, they gradually transformed into a low-melting CaO–MgO–Al_2O_3 system. According to the balance of basic and acidic processes, such liquid slag was difficult to separate from the steel. Guo et al. [41] observed that in GCr15 bearing steel, inclusions form mainly as deoxidation products, initially as MgO–Al_2O_3 and Al_2O_3 and later transform into CaO–MgO–Al_2O_3 and CaO–Al_2O_3 during LF–VD processing. Although the number of inclusions decreases slightly, their nature remains, affecting steel cleanliness. Al-Gahtani et al. [42] reported that in API steels, non-metallic inclusions (mainly Al_2O_3, Ca–Al, and Ca–Mg–Al oxides) form during melting and casting, and their composition, size, and number vary with processing stages, ultimately affecting mechanical properties and hydrogen-induced degradation.

Many studies have been conducted on the control of non-metallic inclusions in steels, and research in this area continues [43–51]. However, there remains a need for a detailed investigation of inclusion formation in scrap-based production of AISI1066 steel.

Most existing studies have been carried out under laboratory or optimized conditions. In real industrial production, however, these processes are significantly more complex. Therefore, developing effective approaches to improve steel quality under actual industrial conditions remains a critical challenge.

MATERIAL AND METHODS

AISI1066 high-carbon structural steel was selected as the material for investigation. The melting process was carried out in a 2000-kg-capacity electric

arc furnace at the "Casting–Mechanical" workshop of JSC "Uzmetkombinat". It is important to note that this grade of steel is widely used in industrial production. At the same time, it is characterized by a structural tendency toward the formation of non-metallic inclusions.

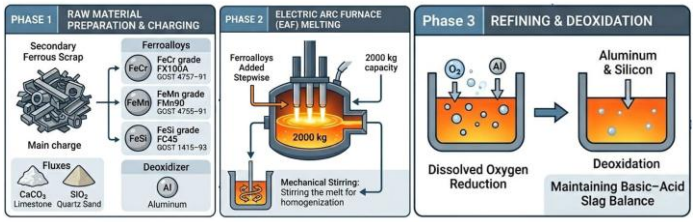

Fig. 1 Schematic representation of the technological process under industrial conditions

The charge material mainly consisted of secondary ferrous scrap. This leads to residual elements in the alloy and to local variations in chemical composition. FX100A (GOST 4757–91), FMn90 (GOST 4755–91) and FC45 (GOST 1415–93) ferroalloys and pure Al were used in the charge composition as alloying and reducing agents. Limestone ($CaCO_3$) and quartz sand (SiO_2) were used as a flux to promote slag formation and improve metal refining efficiency (**Fig. 1**).

The melting process was carried out in an electric arc furnace. Technological parameters, including the temperature regime, degree of melt mixing, and slag–metal interaction, were controlled in accordance with established technological procedures. During melting, ferroalloys were added incrementally to achieve the required chemical composition. Deoxidation was performed using aluminum and silicon, resulting in a reduction of dissolved oxygen in the melt. In addition, the slag composition was controlled through the basicity coefficient. This led to the activation of the coagulation of non-metallic inclusions and their separation from the metal bath.

To ensure uniform distribution of elements in the alloy composition, mechanical stirring was used. After that, the melt was poured from the furnace into a ladle, and liquid alloy samples were taken from three different points of the ladle and cast into pre-prepared molds. This served to ensure the reliability of the research results.

Sample preparation

All experimental samples were prepared in accordance with GOST standards. The cast samples were removed from sand–clay molds and subjected to preliminary cleaning.

Fig. 2 Preparation of the test samples using the Tegramin-30 (Struers, Denmark) equipment

The research samples were machined on a lathe to meet the specified dimensions for testing. The machining process was carried out in the presence of a cooling and lubricating fluid, which prevented overheating of the alloy and preserved its microstructure [52–54].

For metallographic investigations, the samples were prepared using a Struers CitoPress-10 (Struers, Denmark) at 140 °C with thermosetting resin and formed into cylindrical specimens suitable for grinding and polishing.

In the next stage, surface polishing of the research samples was carried out using a Struers Tegramin-30 device (Struers, Denmark). The grinding process was performed using silicon carbide (SiC)-based abrasive papers with sizes of 200, 400, 600, 800, 1000, 1200, and 2000 µm. This stage enabled the removal of deformed surface layers and the attainment of a smooth, defect-free surface (**Fig. 2**).

After grinding, the samples were washed with distilled water. The purpose of this was to remove abrasive residues. Final polishing was performed using a suspension with a particle size of 0.3 µm. After that, the samples were cleaned with ethanol to remove surface contaminants and prevent oxidation.

SEM–EDS

To reveal the microstructure, the specimens were chemically etched using a 1% nital solution (99% ethanol and 1% nitric acid). The etching time was approximately 24 seconds. This treatment enabled clear observation of non-metallic inclusions using optical microscopy and SEM.

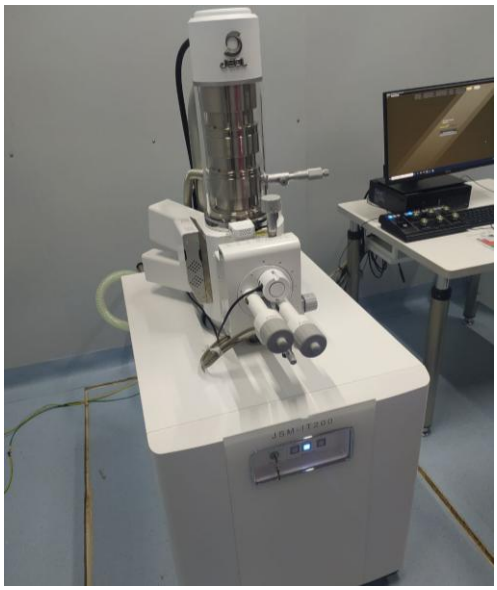

Fig. 3 Investigation of the samples was carried out using the JEOL JSM-IT200 equipment (Jeol, Japan)

Energy-dispersive X-ray spectroscopy (EDS) was used for elemental analysis. Elemental mapping was performed to determine the spatial distribution of elements (**Fig. 3**). The elements examined included Fe, Mn, Si, S, Al, Cr, Ni, Cu, and Mo. The mapping results enabled identification of compositional correlations among elements.

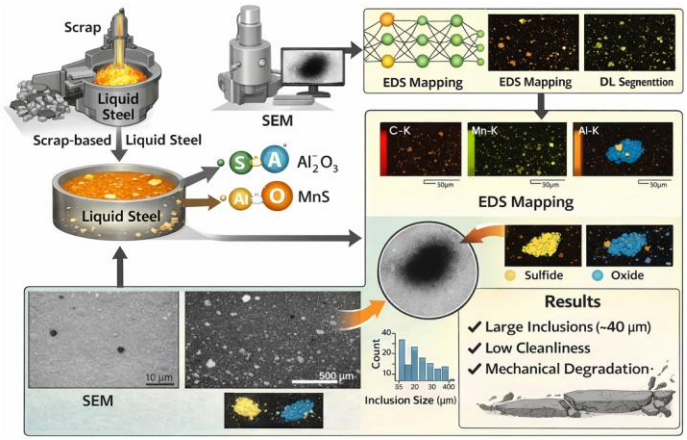

Fig. 4 Experimental workflow diagram for melting in an electric arc furnace, sample preparation, and analysis of non-metallic inclusions using SEM–EDS methods.

Deep learning (DL)-based segmentation model

Based on SEM analyses of the investigated alloy, a deep learning (DL)-based semantic segmentation method was also applied to automatically detect and classify non-metallic inclusions. The implemented model architecture is shown in **Fig. 5**. It is based on a U-Net type convolutional neural network widely used for image segmentation tasks.

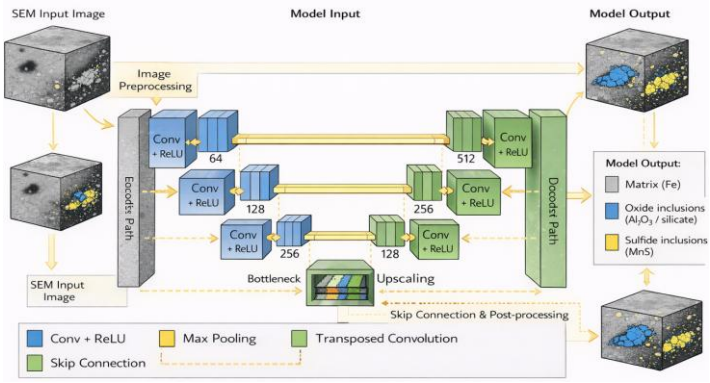

Fig. 5 Structure of the DL model for automatic detection of non-metallic inclusions based on SEM results of the investigated AISI1066 steel sample

The encoder part of the network is responsible for feature extraction. It consists of several convolutional layers. They operate together with nonlinear activation functions and max-pooling operations. By performing a sequential downsampling process, the encoder identifies the hierarchical features of SEM microstructures obtained from the samples. The decoder part performs upsampling to reconstruct the segmented microstructure image from the SEM results. Using transposed convolution layers, the spatial resolution is restored, yielding pixel-level classification maps. Skip connections are applied between the encoder and decoder layers.

The input data for the model consists of processed SEM images of the investigated samples. The model output is a segmentation mask in which each pixel is classified into one of the following categories: metallic matrix, oxide inclusions, and sulfide inclusions.

The segmentation process enables high-accuracy analysis of the morphology, size, and spatial distribution of non-metallic inclusions. This capability is of great importance for reliable analysis of heterogeneous microstructures found in steels based on secondary production.

Compared with conventional manual image analysis, the deep learning (DL) approach offers advantages such as higher accuracy, reduced subjectivity, and faster processing [55,56]. The model enables consistent identification of inclusion boundaries.

Using image analysis techniques, the equivalent diameter of inclusions was calculated. The obtained values were grouped into predefined size intervals, and the statistical distribution of inclusion sizes was presented as a histogram.

RESULTS AND DISCUSSION

Metallographic analysis results

The microstructure of the investigated AISI1066 steel samples was examined at different magnifications using an Axiovert 40 MAT (ZEISS, Germany) metallographic microscope. The observation and analysis results revealed a heterogeneous microstructure comprising secondary phases and non-metallic inclusions within a Fe-based matrix.

In **Fig. 6a** and **Fig. 6d**, at low magnification up to X100, dark boundaries distributed along the grain boundaries are clearly observed in the samples' microstructures. These dark regions are mainly associated with troostite microstructure and boundary segregation of carbide compounds. These accumulations arise from microstructural inhomogeneities, chemical composition-related issues, and thermal effects in the samples.

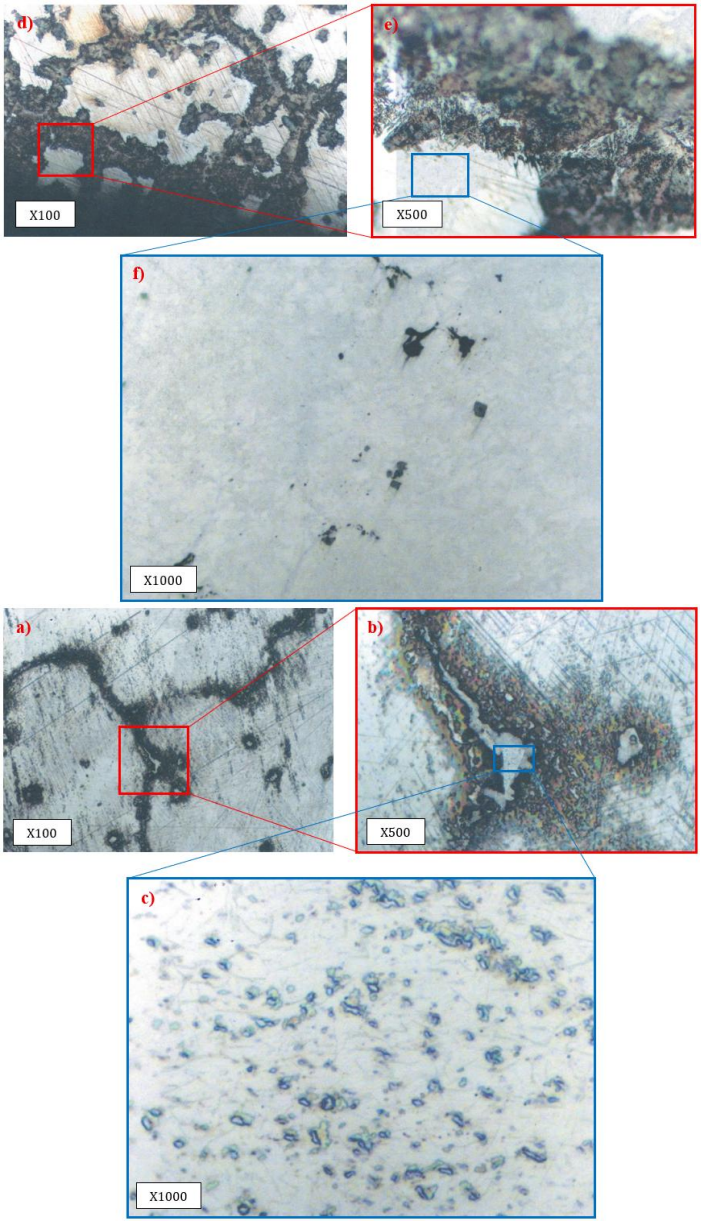

Fig. 6 Metallographic microscope analysis results of the research samples

In **Fig. 6b** and **Fig. 6e**, at medium magnification up to X500, the distribution of secondary phases in the samples' microstructures is shown more clearly. In particular, carbide compounds are distributed non-uniformly and in clusters. In some regions, a high density of these phases is observed. At the same time, the coexistence of non-metallic inclusions and carbide phases in mixed form is also observed in the microstructures. These represent very complex phases. Such heterogeneity indicates that diffusion and segregation processes during solidification of the molten metal in the mold did not proceed properly.

In Fig. 6c, at high magnification up to X1000, non-metallic inclusions and inclusions of sulfide and oxysulfide types in the form of fine dispersed particles are identified in the microstructure. It can be observed that they are non-uniformly distributed throughout the Fe matrix. In some regions, local accumulations are also formed. At the same time, in Fig. 6f, at high magnification up to X1000, another microstructure shows relatively larger non-metallic inclusions along with gas porosity. These casting defects occurred due to gas (O_2, N_2, H_2) evolution during melting in the furnace and pouring into ladles or due to incomplete removal of slag residues. The large non-metallic inclusions and gas porosity remaining in the alloy act as stress concentrators.

In the analyzed optical microstructures, troostite, carbides, non-metallic inclusions, and gas porosity are observed to be unevenly distributed in a mixed form. In particular, their location along grain boundaries forms structurally weakened zones. This creates favorable conditions for crack initiation in cast products or working components. As a result, it decreases the material's fatigue resistance and impact toughness.

SEM–EDS results

The microstructural analysis of the AISI1066 steel sample investigated was conducted using scanning electron microscopy (SEM) at different magnifications to evaluate the morphology, size, and distribution of non-metallic inclusions. The observations revealed a heterogeneous microstructure comprising a continuous iron-based matrix and dispersed secondary phases.

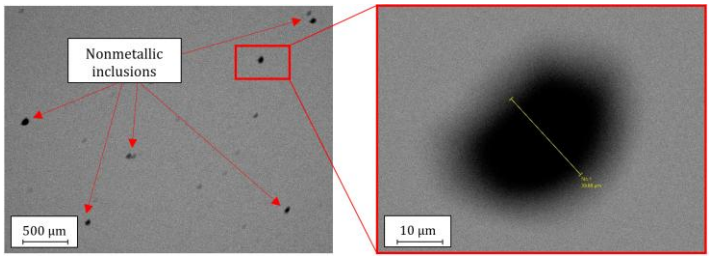

Fig. 7 Non-metallic inclusions and their size in the AISI1066 alloy structure

At magnifications up to X40, the overall structure shows a relatively homogeneous metallic matrix with randomly distributed inclusions. In backscattered electron mode, the inclusions were observed as dark contrast against a bright Fe-rich background. This indicates that they consist of phases with a lower average atomic number. The spatial distribution of inclusions is non-uniform. In some regions, localized clustering was observed. Such clustering is characterized by the fact that inclusion formation is not entirely random. That is, it indicates a relationship with local solidification conditions and the chemical composition of the melt.

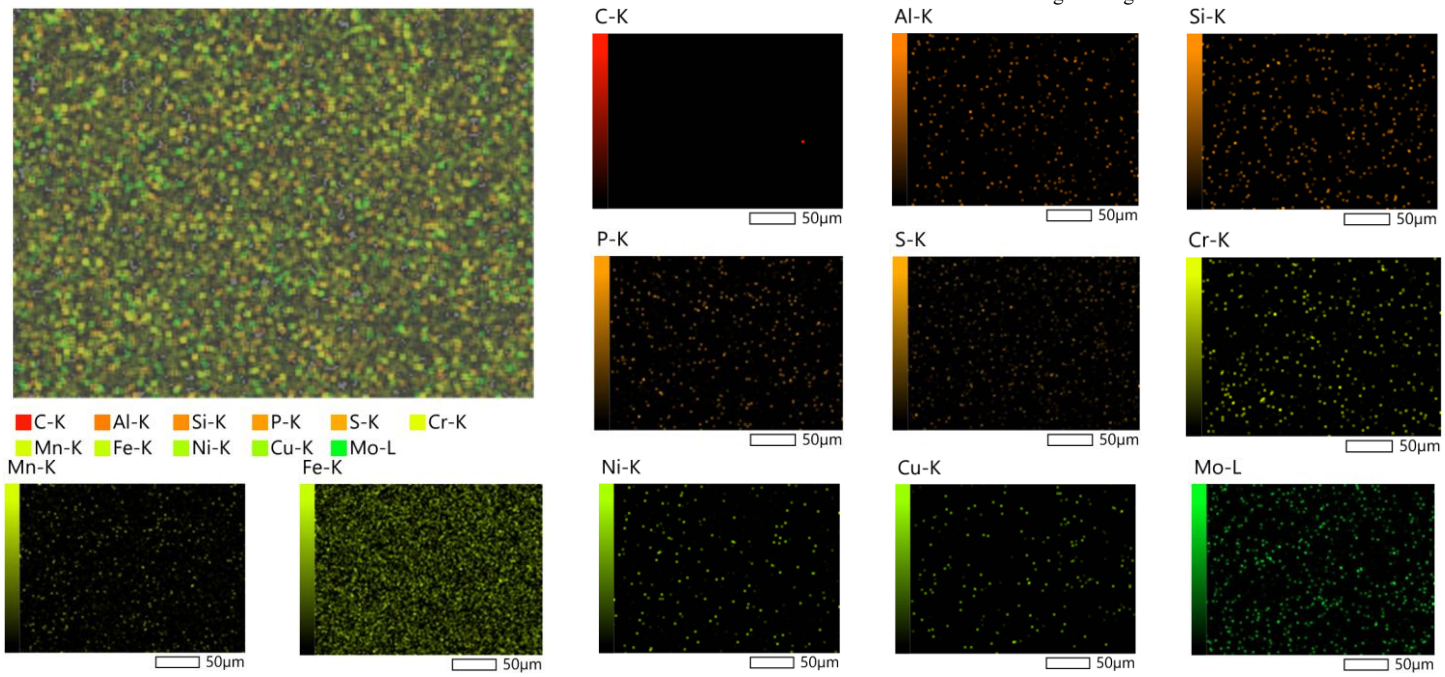

Fig. 8 Spatial distribution of chemical elements in the investigated alloy

At higher magnification up to X1000, the shape and size of the inclusions are more clearly observed. The inclusions are mainly spherical (globular) and irregular in shape, and their sizes range from a few micrometers up to approximately 40 µm (**Fig. 7**). The presence of large-sized inclusions indicates that the steel was not sufficiently refined during the melting process. That is, it is characterized by incomplete removal of non-metallic phases (**Fig. 8**).

It is noteworthy that the inclusions did not exhibit elongated or stringer-like morphology. This type is usually observed in plastically deformed steels. In contrast, their equiaxed and irregular shapes indicate that the material has retained the characteristics of a cast structure. This is consistent with the production technology. Furthermore, it indicates that inclusion modification and directional alignment have not occurred.

In some regions, inclusions with indistinct or diffuse boundaries were also observed. This indicates the formation of complex inclusions as a result of the interaction of several inclusion phases during solidification. Such inclusions consist of a combination of oxides, sulfides, and silicates.

The size distribution of inclusions is of particular importance. Fine inclusions (<10 µm) are generally considered less harmful. However, the presence of coarse inclusions (~40 µm) is a serious metallurgical issue. Such inclusions act as stress concentrators. Especially in components operating under fatigue and impact loading, they can serve as crack initiation sites.

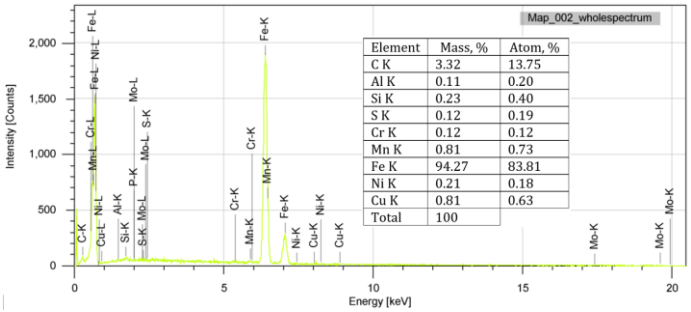

Fig. 9 EDS spectrum of the investigated AISI1066 steel sample.

From a metallurgical point of view, SEM observations showed that the cleanliness level of the investigated steel is relatively low. The heterogeneous distribution of large inclusions and their complex morphology indicate that the control of inclusion formation during melting and solidification was not sufficiently effective. This clearly has a direct negative effect on the mechanical properties of the material.

In addition, the chemical composition of the investigated samples and the elemental volumetric distribution were studied using energy-dispersive X-ray

spectroscopy (EDS). In this case, quantitative analysis and spectral evaluation were applied together.
In the EDS spectrum of the investigated sample presented in **Fig. 9**, the Fe-K peak located in the range of 6–7 keV is clearly observed. In addition, distinct peaks corresponding to Mn, Si, Cr, Ni, and Cu elements are also present. This confirms the quantitative EDS results. The results also confirm the presence of peaks corresponding to C and O in the lower energy regions. This indicates the presence of oxide phases in the composition.
The high sulfur (S) content (0.12 wt.%) in the chemical composition of the investigated samples is significantly higher than the limits specified for quality steels and AISI1066 steel. This promotes the formation of manganese sulfide (MnS) inclusions. That is, the co-presence of Mn and S elements in the regions indicates the formation of MnS phases. These inclusions have a significant negative effect on mechanical properties.
The high copper (Cu) content (0.81 wt.%) is not typically intentionally added to AISI1066 steel. Therefore, its presence is explained by the use of scrap materials. High copper content leads to hot shortness. At the same time, it can also deteriorate hot deformation properties.
At the same time, aluminum (Al) and silicon (Si) elements were detected together with oxygen (based on spectral and mapping data). This indicates the presence of oxide inclusions, including Al_2O_3 and silicate phases. These inclusions are formed during deoxidation processes both inside and outside the furnace. If they are not completely removed from the melt, they remain in the metal during solidification. The coexistence of sulfide and oxide phases indicates the formation of complex non-metallic inclusions. This is considered harmful due to their heterogeneous structure and large size.

Deep learning (DL)-based segmentation analysis

The results of deep learning-based segmentation are presented in **Fig. 10**. The figure shows the model dividing the SEM image into the metallic matrix, oxide inclusions, and sulfide inclusions. The results obtained are consistent with the morphology observed in SEM images and the compositional trends identified by EDS analysis.

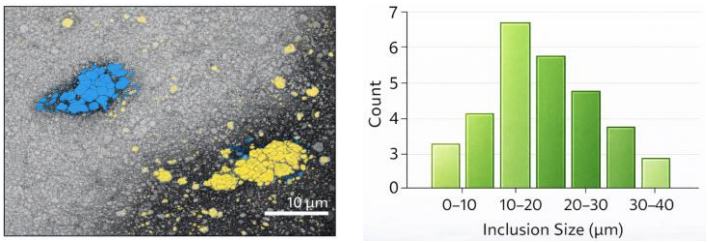

a) b)

Fig. 10 a) Result of the model analysis of the SEM image based on deep learning (DL). At a scale of 10 µm, it is divided into oxide phases in blue and sulfide-type non-metallic phases in yellow; b) Histogram of inclusion size distribution in the range up to ~40 µm

One important observation from the segmentation results is the clear distinction between coarse and finely dispersed particles. The model classifies inclusions with sizes ≥30 µm mainly as oxide phases.
In contrast, fine inclusions are relatively uniformly distributed. They are mainly identified as sulfide phases. These types of non-metallics have smoother morphology and are usually associated with sulfur segregation during the final stages of solidification. The model's ability to distinguish these types demonstrates its sensitivity in identifying morphological and textural features.
In addition, fine particles are clustered in certain regions, while coarse inclusions occur separately. This non-uniform distribution indicates that local thermodynamic and kinetic conditions in the melt influence the formation of inclusions. From a quantitative perspective, Fig. 10b shows that segmentation clearly separates inclusion boundaries.
An important aspect is that the segmentation results are consistent with EDS-based compositional analysis. That is, the co-occurrence of Mn and S elements confirms sulfide inclusions, while Al and Si confirm oxide phases. This agreement demonstrates the model's classification accuracy.

Classification of non-metallic inclusions

Based on SEM observations and EDS analyses of the investigated samples, non-metallic inclusions were classified into several main categories based on their chemical composition, morphology, and sources of formation. Understanding the mechanisms of inclusion formation is important for evaluating their effects on the alloy's physical–mechanical properties.
The relatively high sulfur content (0.12 wt.%) in the sample significantly promotes the formation of manganese sulfide (MnS). SEM observations show that MnS inclusions are spherical and distributed within the matrix. Elongated (stringer) forms typical of deformed steels were not observed.
The formation of oxide inclusions is mainly associated with aluminum and silicon, which are used as deoxidizing elements during the steelmaking process. EDS analyses confirm the formation of oxide phases belonging to Al_2O_3 and SiO_2 types, and they have a lower atomic number compared to the iron matrix. Therefore, they appear as dark, irregularly shaped particles. This indicates that deoxidation products were not completely removed from the melt during melting. That is, it may be related to insufficient flotation processes and inefficient slag–metal separation. At the same time, it may also be associated with insufficient ladle treatment outside the furnace.
Oxide inclusions have high hardness and brittleness. Therefore, they are considered more harmful than sulfides. During service, they act as stress concentrators, which significantly reduces fatigue resistance and impact toughness of the components (**Fig. 11**).
One important result of the study is the presence of complex inclusions. The analysis of the obtained SEM observations shows that some inclusions have diffuse boundaries. This indicates that these compounds observed in the alloy composition have a multiphase structure. Analysis of the EDS results also confirms the coexistence of Manganese (Mn), Sulfur (S), Aluminium (Al), and Silicon (Si) in the same region. This suggests that oxide particles act as nucleation sites for sulfides. As a result, complex composite non-metallic inclusions are formed.
The above analyses confirm the presence of oxide, sulfide, and complex inclusions in the investigated steel.

Formation mechanism of inclusions and their effect on mechanical properties

The formation of non-metallic inclusions occurs as a result of complex physicochemical processes taking place during melting, deoxidation, and solidification. The situation observed in the investigated sample is directly related to these processes. Based on SEM–EDS observations, the formation mechanism of inclusions is interpreted as a multi-stage process. In this process, the formation of oxides, the precipitation of sulfides, and interphase interactions play important roles.
The formed oxides are dispersed in the liquid alloy as fine particles under high-temperature conditions. However, under real conditions, these particles should rise and be removed into the slag. The simultaneous detection of Al, Si, and oxygen indicates that this process was not fully completed. As a result, these particles act as nucleation sites for the formation of further inclusions.
Since sulfur has low solubility in the solid phase, it accumulates in the remaining liquid phase during solidification. The sufficient presence of manganese (0.81 wt.%) leads to the formation of MnS inclusions.
The sulfur content of 0.12 wt.% further intensifies this process, and they are typically formed in interdendritic regions.
One of the main results of the study is the formation of complex inclusions. Such inclusions form as a result of interactions between oxide and sulfide phases.
Fine oxide particles such as Al_2O_3 and silicates serve as heterogeneous nucleation sites for MnS. During solidification, sulfur and manganese diffuse toward these particles, forming composite inclusions.
The presence, size, morphology, and distribution of non-metallic inclusions are important factors determining the quality of steels. In the investigated AISI1066 steel, sulfides (MnS), oxides (Al_2O_3, SiO_2), and complex multiphase inclusions are present. This clearly has a negative effect on the mechanical properties of this alloy.

DISCUSSION

There is a difference between these non-metallic inclusions and the metallic matrix in terms of mechanical properties. This difference serves as stress

concentrators. That is, oxide inclusions are highly hard and brittle. Therefore, they have weak bonding with the Fe matrix. Under external loading in working components, these interfaces become the most favorable sites for crack initiation.

are primarily oxide phases, whereas fine inclusions (<20 µm) are primarily sulfide phases. The agreement of these results with SEM and EDS analyses confirms the accuracy of the model.

Based on the size distribution histogram, the majority of inclusions are located in

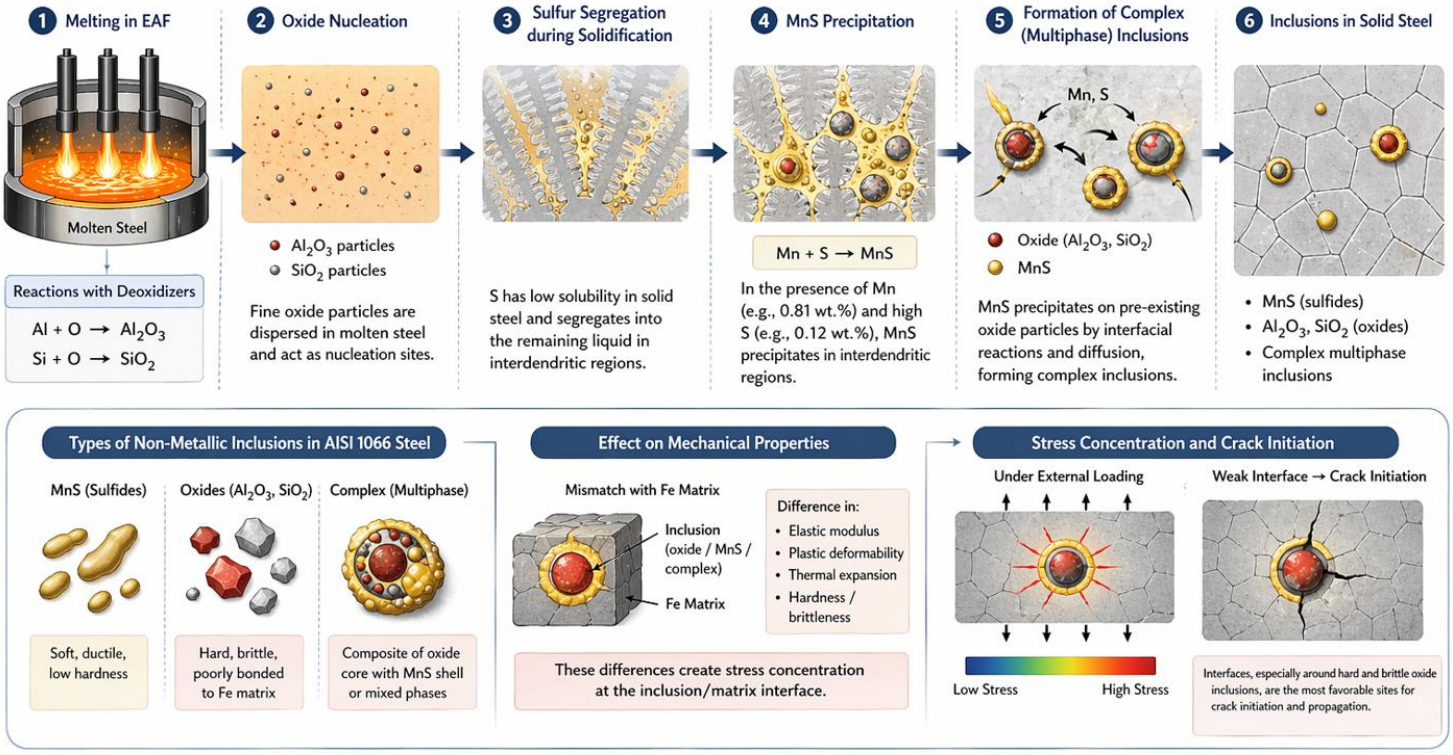

Fig. 11 Formation mechanism of non-metallic inclusions and their effect on mechanical properties in research sample steel AISI1066

Based on the results of SEM–EDS analysis, it can be stated that sulfides, oxides, and complex multiphase particles are present in the investigated AISI1066 steel.

In secondary metallurgy processes, significant reduction in the size of non-metallic inclusions and improvement of their morphology in the alloy can be achieved by applying methods such as secondary refining, argon stirring, and calcium treatment [21–34, 57,58,59].

The results show that the identified coarse, complex, and non-uniformly distributed inclusions are related to the limitations of scrap-based melting. According to the analysis of the study, the investigated material has a low level of cleanliness. This is expected to negatively affect its mechanical properties.

CONCLUSION

In this study, the formation, composition, and effect of non-metallic inclusions in AISI1066 steel alloy obtained by melting secondary metal scrap in an electric arc furnace were analyzed using combined SEM–EDS and deep learning (DL)-based segmentation methods. Based on the obtained results, the following conclusions were drawn:

Non-metallic inclusions unevenly distributed in the Fe-based matrix were identified in the alloy microstructure. Their sizes ranged from a few micrometers up to ~40 µm. The presence of such large inclusions indicates that the investigated alloy has a low level of cleanliness.

The analysis of the research proved that MnS, Al_2O_3, SiO_2, as well as gas porosity, are concentrated in one region of the alloy and have formed non-metallic inclusions and phases consisting of complex multiphase particles. The sulfur content of 0.12 wt.% and manganese content of 0.81 wt.% in the samples led to an increase in the natural formation of MnS. The copper content of 0.81 wt.% indicates contamination from the uncontrolled composition of secondary metal scrap.

The deep learning-based segmentation results enabled automatic detection and classification of inclusions. The results showed that coarse inclusions (≥30 µm) the range of 10–25 µm. However, the presence of coarse inclusions in the range of 30–40 µm was also identified. This distribution was shown to have a right-skewed character.

The mechanism of non-metallic inclusion formation during secondary melting was explained by the initial formation of oxides during deoxidation, followed by the precipitation of MnS sulfides during solidification and their interaction leading to the formation of complex inclusions.

The identified coarse oxide inclusions up to ~40 µm act as stress concentrators.

Acknowledgements: The authors express their deep gratitude to JSC "Uzmetkombinat" production enterprise for their support in carrying out the experimental work.

REFERENCES

1. Jia, X., Yang, Y. L., Ma, Y., & Wang, B. X. (2023). Effect of Oxide Metallurgy Technology on Mechanical Properties and Hydrogen-Induced Cracking Susceptibility of High-Strength Low-Alloy Steel. *Steel Research International*, *94*(5), 2200320. https://doi.org/10.1002/srin.202200320
2. Cai, C., & Mu, W. (2025). Utilization of Non-Metallic Inclusion to Induce Intragranular Acicular Ferrite Formation Contributing to "Oxide Metallurgy": Effect of Ti/Al Content on the Microstructure Evolution. *Steel Research International*, *96*(8), 2400360. https://doi.org/10.1002/srin.202400360
3. Luo, Y., Du, J., Liu, B., He, W., Ji, C., Yuan, L., & Li, H. (2025). Regulating Non-metallic Inclusions with Pulsed Electric Current in Ultra-Low Carbon Steel and Industrial Practice. *Metallurgical and Materials Transactions B: Process Metallurgy and Materials Processing Science*, *56*(6), 6508–6515. https://doi.org/10.1007/s11663-025-03782-7
4. Chan, K. S. (2010). Roles of microstructure in fatigue crack initiation. *International Journal of Fatigue*, *32*(9), 1428-1447. https://doi.org/10.1016/j.ijfatigue.2009.10.005

5. Holappa, L., & Wijk, O. (2024). Inclusion Engineering. In *Treatise on Process Metallurgy: Industrial Processes*: Vol. 3, Second Edition, 303-321. https://doi.org/10.1016/B978-0-323-85373-6.00015-6
6. Tursunbaev, S., Turakhodjaev, N., Zhang, L., Wang, Z., Mardonov, U., & Saidova, M. (2024). Mechanical properties and evolution of the microstructure of al-cu-mg system alloys under the influence of alloying elements (ge and si). *International Journal of Mechatronics and Applied Mechanics*, *2024*(18), 164-169. https://doi.org/10.17683/ijomam/issue18.19
7. Tursunbaev, S., Turakhujaeva, A., Mardonov, U., Mardonakulov, S., Saidova, M., Murodqosimov, R., & Kudratkhodjaeva, N. (2025). Analysing the alternations in the aluminium alloy properties under the influence of silicon and germanium alloying elements. *International Journal of Mechatronics and Applied Mechanics*, *1*(21), 365-372. https://doi.org/10.17683/ijomam/issue21.34
8. Narivskyi, A. V., Smirnov, O. M., Tarasevich, M. I., Kondratyuk, S. Ye., & Perekhoda, V. V. (2020). Non-metallic inclusions in the large blacksmith ingot made from steel 25ХН3МФА. *Metal and Casting of Ukraine*, *28*(4), 14. https://doi.org/10.15407/steelcast2020.04.014
9. Krechkovska, H.V., Solovei, P.R., & Student, O.Z. (2025). Effect of non-metallic inclusions in steel structure on the premature failure of the steam turbine rotor disk. *Materials Science*, *61*(1), 66–72. https://doi.org/10.1007/s11003-025-00962-3
10. Kholmirzaev, N., Saidmakhamadov, N., Khasanov, J., Tadjiev, N., Yusupov, B., Sadikova, N., Yuldashev, O., Makhmudov, F., Nosirkhujaev, I. S., & Nurdinov, Z. (2024). Mathematical Modeling of the Effect of TiC Nanopowder Particles on the Wear Resistance Properties of Low-Alloy Steel. In *Materials Science Forum*, 1139, 11-19. https://doi.org/10.4028/p-gIS27O
11. Milovanović, V., Dunić, V., Rakić, D., & Živković, M. (2013). Identification causes of cracking on the underframe of wagon for containers transportation - Fatigue strength assessment of wagon welded joints. *Engineering Failure Analysis*, *31*, 118-131. https://doi.org/10.1016/j.engfailanal.2013.01.039
12. Park, J. H., & Zhang, L. (2020). Kinetic Modeling of Nonmetallic Inclusions Behavior in Molten Steel: A Review. In *Metallurgical and Materials Transactions B: Process Metallurgy and Materials Processing Science*, 51(6), 2453–2482. https://doi.org/10.1007/s11663-020-01954-1
13. Zhang, L., & Pluschkell, W. (2003). Nucleation and growth kinetics of inclusions during liquid steel deoxidation. *Ironmaking and Steelmaking*, *30*(2). https://doi.org/10.1179/030192303225001766
14. Peng, W., Chen, Z., Yan, W., Chen, J., Li, G., & Li, Y. (2024). Microstructure and properties of ceramic filter containing porous MgO coating and its filtration of Al2O3 inclusions in molten steel. *Ceramics International*, *50*(1), 218-229. https://doi.org/10.1016/j.ceramint.2023.10.096
15. Storti, E., Kerber, F., Dudczig, S., Wagner, R., Weidner, A., Biermann, H., & Aneziris, C. G. (2023). Combined steel melt filtration through reactive and active filters. *Open Ceramics*, *15, 100415*. https://doi.org/10.1016/j.oceram.2023.100415
16. Saidmakhamadov, N., Kholmirzaev, N., Bekchanova, V., Odilov, F., Tukhtaboev, I., Gaybullaev, M., Gulyamov, S., & Eshimov, D. (2025). Mathematical modeling of the influence of the gating system on the quality of the cast product during alloy casting. *AIP Conference Proceedings*, *3268*(1), 030002. https://doi.org/10.1063/5.0257618
17. Khasanov, J., Kholmirzaev, N., Saidmakhamadov, N., Tojiboev, B., Dilshodbek, E., Makhammadjanov, K., Bektemirov, A., Arabbaeva, F., & Otakuziev, A. (2024). Development of technology for obtaining thin-walled details from gray cast iron in sand-clay moulds. *International Journal of Mechatronics and Applied Mechanics*, *2024*(18), 199-209. https://doi.org/10.17683/ijomam/issue18.24
18. Kim, W. Y., Nam, G. J., & Kim, S. Y. (2021). Evolution of Non-Metallic Inclusions in Al-Killed Stainless Steelmaking. *Metallurgical and Materials Transactions B: Process Metallurgy and Materials Processing Science*, *52*(3), 1508–1520. https://doi.org/10.1007/s11663-021-02119-4
19. She, C., Zhu, L., Ren, Y., Sun, Y., & Zhang, L. (2025). Control of steel cleanliness and non-metallic inclusions in an Al-killed steel through CaO-Al2O3 powder injection during RH refining process. *Metallurgical Research and Technology*, *122*(4), 401. https://doi.org/10.1051/metal/2025031
20. Zhang, X., Ye, Z., Wang, J., Wang, W., Zhang, H., & Zhang, L. (2025). Control of non-metallic inclusions and micro-structure of an Al-killed steel through adjusting titanium content. *Journal of Materials Research and Technology*, *35, 181*. https://doi.org/10.1016/j.jmrt.2025.02.181
21. Podder, A., Coley, K. S., & Phillion, A. B. (2024). Simulation of Ladle Refining Reactions in Si–Mn-Killed Steel. *Steel Research International*, *95*(5), 2300330. https://doi.org/10.1002/srin.202300330
22. Guo, X., Godinez, J., Walla, N. J., Silaen, A. K., Oltmann, H., Thapliyal, V., Bhansali, A., Pretorius, E., & Zhou, C. Q. (2021). Computational investigation of inclusion removal in the steel-refining ladle process. *Processes*, *9*(6), 1048. https://doi.org/10.3390/pr9061048
23. Deng, X. cong, Wei, K. xian, Ma, W. hui, Tang, Q. wei, & Zhang, H. (2023). Separation of phosphorus from metallurgical-grade silicon via micro negative pressure during oxidative ladle refining. *Transactions of Nonferrous Metals Society of China (English Edition)*, *33*(4), 1296-1304. https://doi.org/10.1016/S1003-6326(23)66183-7
24. Arinova, S., Kulikov V., Kvon, S., & Altynova, A. (2025). Studying the Compositions and Modes of Manufacturing Refractory Products Using Steel Production Slag. *Acta Metallurgica Slovaca, 31(2), 74–77*. https://doi.org/10.36547/ams.31.2.2153
25. Ślęzak, M., Migas, P., & Czech, A. W. (2024). High-Temperature Rheometric and Melting Experiments of Refining-Type Ladle Slag Systems. *JOM*, *76*(8), 4445–4457. https://doi.org/10.1007/s11837-024-06646-8
26. Tang, H. yan, Li, J. she, Xie, C. hong, Yang, S. feng, Sun, K. ming, & Wen, D. song. (2009). Rational argon stirring for a 150-t ladle furnace. *International Journal of Minerals, Metallurgy and Materials*, *16*(4), 383-386. https://doi.org/10.1016/S1674-4799(09)60068-6
27. Cheng, G., Zhang, L., Ren, Y., Yang, W., Zhao, X., & Wang, G. (2021). Evolution of Nonmetallic Inclusions with Varied Argon Stirring Condition during Vacuum Degassing Refining of a Bearing Steel. *Steel Research International*, *92*(1), 2000364. https://doi.org/10.1002/srin.202000364
28. Lu, H., Cheng, Q., Zhong, Y., Cheng, C., Ren, W. L., Ren, Z., & Lei, Z. (2025). Analysis of Flow Pattern and Bubble Behavior in Slab Continuous Casting with Mold Electromagnetic Stirring. *Steel Research International*, *96*(3), 2400591. https://doi.org/10.1002/srin.202400591
29. Ahmad, H., Tang, F., Yao, Z., Xu, Y., Huang, Z., Zhao, B., & Ma, X. (2023). Formation and Modification of Al2O3 and MnS Inclusions in Al-Killed Gear Steels via Ca Treatment. *Metals*, *13*(7), 1153. https://doi.org/10.3390/met13071153
30. Valanezahad, A., Ishikawa, K., Tsuru, K., Maruta, M., & Matsuya, S. (2011). Hydrothermal calcium modification of 316L stainless steel and its apatite forming ability in simulated body fluid. *Dental Materials Journal*, *30*(5), 153. https://doi.org/10.4012/dmj.2010-153
31. Sidorova, E., Karasev, A. v., Kuznetsov, D., & Jönsson, P. G. (2019). Modification of non-metallic inclusions in oil- pipeline steels by ca-treatment. *Metals*, *9*(4), 391. https://doi.org/10.3390/met9040391
32. Ren, Y., Wang, W., Yang, W., & Zhang, L. (2023). Modification of Non-metallic Inclusions in Steel by Calcium Treatment: A Review. In *ISIJ International*, 63(12), 1927-1940. https://doi.org/10.2355/isijinternational.ISIJINT-2023-143
33. Zhong, H., Jiang, M., Luan, B., Ren, X., & Wang, X. (2025). Modifications of Inclusions in Ca-Treated and Mg-Treated Pipeline Steel Melts. *Metallurgical and Materials Transactions B: Process Metallurgy and Materials Processing Science*, *56*(4), 4170–4185. https://doi.org/10.1007/s11663-025-03590-z
34. Hu, S. qin, Zheng, W., Liu, D. yao, Yan, Z. rui, Li, G. qiang, Liu, J., & Huang, F. (2025). Inclusion Modification and Evolution during Reheating of Ca-Treated Ti–Al–Mg Deoxidized High-Strength Low-Alloy Steels with Two Different Ti/Al Content Ratios. *Steel Research International*, *96*(10), 550-563. https://doi.org/10.1002/srin.202401083
35. Kholmirzaev, N., Turakhodjaev, N., Saidmakhamadov, N., Tadjiev, N., Khasanov, J., Yusupov, B., Khojibekova, S., Sadikova, N., Nosirkhujaev, I. S., & Juraev, J. (2024). Improvement of the Technology of Melting of Low Alloy Steel Alloy in an Electric Arc Furnace. *Materials Science Forum,* 1139, 3-9. https://doi.org/10.4028/p-2AMBsZ
36. Kholmirzaev, N., Khasanov, J., Abdullayev, B., Saidkhodjaeva, S., Bektemirov, A., Sadikova, N., Yusupov, B., Nosirkhujaev, I. S., & Nurdinov, Z. (2024). Improving the technology of obtaining highquality castings from steel in sand-clay molds. *E3S Web of Conferences*, *525, 3012*. https://doi.org/10.1051/e3sconf/202452503012
37. Dobosz, A., Spychaj, S., & Karbowniczek, M. (2024). *The Steel Scrap Purity Analysis in the Context of the Quality of Steel Produced at AMW*. https://doi.org/10.3390/proceedings2024108019
38. Dworak, S., Rechberger, H., & Fellner, J. (2022). How will tramp elements affect future steel recycling in Europe? – A dynamic material flow model for

steel in the EU-28 for the period 1910 to 2050. *Resources, Conservation and Recycling*, *179, 106072*. https://doi.org/10.1016/j.resconrec.2021.106072
39. Wang, Y., Lin, S., Dong, Z., Park, J. H., Wang, Q., Ni, H., & Mu, W. (2023). Characterization and formation mechanism of non-metallic inclusions in single bcc-phase high entropy alloy. *Materials Characterization*, *205, 113299*. https://doi.org/10.1016/j.matchar.2023.113299
40. Qiao, T., Cheng, G., Huang, Y., Li, Y., Zhang, Y., & Li, Z. (2022). Formation and Removal Mechanism of Nonmetallic Inclusions in 42CrMo4 Steel during the Steelmaking Process. *Metals*, *12*(9), 1505. https://doi.org/10.3390/met12091505
41. Guo, Z., Lou, X., Wang, J., Liu, E., Wang, Q., Liu, Z., Wang, L., & Zhu, L. (2025). Characterization and evolution of non-metallic inclusions in GCr15 bearing steel during refining process. *Ironmaking and Steelmaking*. https://doi.org/10.1177/03019233251353543
42. Al-Gahtani, M., Pillai, S., & Al-Raddadi, A. (2018). Characterization of non-metallic inclusions in API steel grades using automated energy dispersive X-ray. *Materials Science Forum*, *916, 217*. https://doi.org/10.4028/www.scientific.net/MSF.916.217
43. Hebsur, M. G. (1981). Improved hot workability by control of non-metallic inclusions in steels. *Journal of Applied Metalworking*, *2*(1). https://doi.org/10.1007/BF02833997
44. Tomita, Y. (1993). Improved fracture toughness of ultrahigh strength steel through control of non-metallic inclusions. *Journal of Materials Science,* 28(4). https://doi.org/10.1007/BF00400864
45. Jiang, M., Wang, X. H., & Wang, W. J. (2010). Control of non-metallic inclusions by slag-metal reactions for high strength alloying steels. *Steel Research International*, *81*(9), 759-765. https://doi.org/10.1002/srin.201000065
46. Da Costa E Silva, A. L. V. (2018). Non-metallic inclusions in steels - Origin and control. *Journal of Materials Research and Technology,* 7(3), 283-299. https://doi.org/10.1016/j.jmrt.2018.04.003
47. Morozov, A.O., Pogodin, A.M., Komolova, O.A., Bikin, K.B., & Grigorovich, K.V. (2020). Control of oxide non-metallic inclusions in production of IF steel. *Izvestiya Ferrous Metallurgy*, *63*(10), 782-790. https://doi.org/10.17073/0368-0797-2020-10-782-790
48. Zhu, M., & Deng, Z. (2022). Evolution and Control of Non-Metallic Inclusions in Steel During Secondary Refining Process. *Jinshu Xuebao/Acta Metallurgica Sinica*, 58(1), 227. https://doi.org/10.11900/0412.1961.2021.00227
49. Zhitenev, A., Karasev, V., Fedorov, A., Ryaboshuk, S., & Alkhimenko, A. (2023). Control of the Composition and Morphology of Non-Metallic Inclusions in Superduplex Stainless Steel. *Materials*, *16*(23), 7337. https://doi.org/10.3390/ma16237337
50. Eckhardt, D. (2025). *Control of non-metallic inclusions in al-killed steels - Inclusion Management, In.: 42º Seminário de Aciaria, Salvador, 2011, 343-354*. https://doi.org/10.5151/2594-5300-18146
51. Zhang, L., & Ren, Y. (2025). Handbook of Non-Metallic Inclusions in Steels. In *Handbook of Non-Metallic Inclusions in Steels*. https://doi.org/10.1007/978-981-97-9638-0
52. Mardonov, U., Madaminov, S., Jeltukhin, A., & Meliboev, Y. (2026). The Influence of Magnetically Treated Lubricating-cooling Fluids on Turning AISI 1045. *Journal of Engineering and Technological Sciences*, *58*(2), 5. https://doi.org/10.5614/j.eng.technol.sci.2026.58.2.5
53. Khasanov, S., Mardonov, U., Ongboyev, A., & Ismatov, M. (2024). Influence of a magnetic field on hss tool wear/life and the intensity of external machining environments in turning. *International Journal of Mechatronics and Applied Mechanics*, *2024*(16), 19. https://doi.org/10.17683/ijomam/issue16.19
54. Mardonov, U., Khasanov, O., Yang, Y., Yatskevich, O., Akramov, M., & Abdullaev, B. (2025). Studying the effect of diverse lubricating and cooling environments in turning gray cast iron. *International Journal of Mechatronics and Applied Mechanics*, *11*(22), 213-223. https://doi.org/10.17683/ijomam/issue22.v2.22
55. Zhang, Y., Zhou, J., Wang, N., Yan, H., Gao, W., Wang, J., Tang, L., Zhang, Y., & Zhang, Z. (2024). Spatiotemporal prediction and characterization of microstructure evolution during in-situ heat treatment using a deep learning algorithm. *Materials Today Nano*, *26, 100471*. https://doi.org/10.1016/j.mtnano.2024.100471
56. Napte, K., & Mahajan, A. (2022). Deep Learning based Liver Segmentation: A Review. *Revue d'Intelligence Artificielle*, *36*(6), 979-984. https://doi.org/10.18280/ria.360620
57. Apelian, D., Mutharasan, R., & Ali, S. (1985). Removal of inclusions from steel melts by filtration. *Journal of Materials Science*, *20*(10), 3501-3514. https://doi.org/10.1007/BF01113756
58. Lipinski, T., Pietraszek, J., & Wach, A. (2022). Influence of oxygen content in medium carbon steel on bending fatigue strength. *Engineering for Rural Development*, *21, 351-356*. https://doi.org/10.22616/ERDev.2022.21.TF116
59. Batista, R. P., Martins, A. A., & Costa e Silva, A. L. V. (2017). The effects of deoxidation practice on the quality of thin foil low-carbon steel. *Journal of Mining and Metallurgy, Section B: Metallurgy*, *53*(3), 357-363. https://doi.org/10.2298/JMMB170730047P